

## Electric Potential Distribution and Short-Range Screening in Nanoporous TiO Electrodes

Arie Zaban, Andreas Meier, and Brian A. Gregg

*J. Phys. Chem. B*, **1997**, 101 (40), 7985-7990 • DOI: 10.1021/jp971857u

Downloaded from <http://pubs.acs.org> on December 4, 2008

### More About This Article

Additional resources and features associated with this article are available within the HTML version:

- Supporting Information
- Links to the 15 articles that cite this article, as of the time of this article download
- Access to high resolution figures
- Links to articles and content related to this article
- Copyright permission to reproduce figures and/or text from this article

[View the Full Text HTML](#)



ACS Publications  
High quality. High impact.

# Electric Potential Distribution and Short-Range Screening in Nanoporous TiO<sub>2</sub> Electrodes

Arie Zaban, Andreas Meier, and Brian A. Gregg\*

National Renewable Energy Laboratory, 1617 Cole Blvd., Golden, Colorado 80401-3393

Received: June 5, 1997; In Final Form: August 4, 1997<sup>⊗</sup>

Impedance spectroscopy and electrochemical dye desorption experiments were employed to study the electrical characteristics of nanoporous TiO<sub>2</sub> electrodes in the dark. The results show an unusual potential distribution across the TiO<sub>2</sub> films, caused by the semiconducting nature of the TiO<sub>2</sub> and the ion motion through the porous film that neutralizes applied electric fields over a short range. These results may have several implications for the functioning of dye-sensitized solar cells: (1) The potential of much of the TiO<sub>2</sub> film will not necessarily correspond to the potential applied to the substrate electrode. (2) Charge carrier motion through the TiO<sub>2</sub> is expected to occur primarily via diffusion rather than drift. (3) The transient electric field generated upon illumination will be quickly neutralized under steady state conditions, but may be an important factor in transient measurements. (4) Systems without excess supporting electrolyte, such as some solid state versions of the dye-sensitized cells, may not be able to efficiently neutralize the field generated by photoinduced charge separation, leading to enhanced charge recombination.

## Introduction

Recent studies of dye-sensitized photoelectrochemical solar cells report light to energy conversion efficiencies as high as 10%.<sup>1–3</sup> Although photosensitization of wide bandgap semiconductors has been studied since the early 1970s,<sup>4–6</sup> high efficiencies were achieved only when nanoporous TiO<sub>2</sub> electrodes were introduced by Grätzel et al.<sup>1</sup> The current increasing research effort in this field is evident from the literature. Reports concerning the basic understanding of the system,<sup>7–11</sup> research toward higher efficiencies and solid-state versions of these cells,<sup>12–14</sup> sensitization of other high surface area semiconductors,<sup>15,16</sup> and new applications such as self-powered electrochromic windows<sup>17,18</sup> and light-emitting diodes<sup>19</sup> have appeared recently.

Despite the high level of activity, a comprehensive fundamental understanding of the system has not been achieved yet. One of the more puzzling components of the dye-sensitized cell is the high surface area TiO<sub>2</sub> electrode. The low absorbance of dye monolayers and the low efficiency of dye multilayers necessitate the use of these high surface area electrodes. However, the resulting porous geometry introduces special characteristics that differentiate these electrodes from their compact analogues. The porous electrodes are strongly influenced by several factors: the open structure of the electrodes that permits electrolyte penetration through the entire electrode; the small size of the individual colloidal particles that cannot support a high space charge; and the low inherent conductivity of TiO<sub>2</sub>.

Various studies were aimed at the characterization of nanoporous TiO<sub>2</sub> electrodes. These studies addressed topics such as the mobility and trapping of photoinduced electrons in the TiO<sub>2</sub> film,<sup>20–22</sup> band position and depletion layer at the semiconductor–liquid interface,<sup>23,24</sup> optical and electrochemical processes at negative bias,<sup>25–27</sup> and the conductivity of porous TiO<sub>2</sub>.<sup>28,29</sup> However, to the best of our knowledge, the potential distribution across the TiO<sub>2</sub> electrodes has not yet been clarified. It is often assumed that the effective potential at any point along the electrode is simply equal to the potential applied to the substrate.<sup>20–27</sup> Since any potential-dependent investigation of

these electrodes has to account for differences between the applied potential and the potential that actually appears at any point along the electrode, it is important to explore the relationship between the two.

We report here impedance spectroscopy and electrochemical dye desorption measurements that suggest that the applied potential is unequally distributed throughout the high surface area TiO<sub>2</sub>–electrolyte interface. For moderate applied bias, the effective potential was found to be equal to the applied potential only in the conducting substrate and in the few TiO<sub>2</sub> layers next to it. The effect of the applied bias decreases as the distance from the substrate increases, because ion motion through the film neutralizes the applied field over a short range. These results suggest that the usual models of the semiconductor–electrolyte interface are not applicable to nanoporous TiO<sub>2</sub> electrodes. For example, standard Mott–Schottky analyses of these semiconductors may appear to be valid, but when the spatial distribution of the potential is taken into consideration, the interpretation of the results may be altered. Furthermore, our results provide a better understanding of dye-sensitized solar cells. For example, when the short-range screening of electric fields in the TiO<sub>2</sub> film is considered, it is clear that charge motion through the film should occur primarily by diffusion rather than by drift. Both the electrode characteristics and their implications to dye-sensitized solar cells will be discussed.

## Experimental Section

**TiO<sub>2</sub> Electrodes.** Three types of electrodes were used in this study: (1) uniform 0.5–9 μm TiO<sub>2</sub> films deposited on conductive SnO<sub>2</sub> glass; (2) TiO<sub>2</sub> films with a thickness gradient, also coated on conductive glass; and (3) uniform 4 μm films on nonconductive microscope slides with an evaporated Ag electrical contact at one end. Conductive glass (Libby Owens Ford, 8 ohm/square F-doped SnO<sub>2</sub>) and the microscope slide substrates were cleaned by overnight immersion in a solution of KOH in 2-propanol, rinsed with deionized water, and dried in a nitrogen stream. All electrodes were made from TiO<sub>2</sub> colloidal suspension (colloid preparation is reported elsewhere<sup>7</sup>) that was spread over the substrate with a glass rod using adhesive tape as spacers. A gradient of spacers was employed to produce the TiO<sub>2</sub> thickness gradient of type 2 electrodes.

\* Corresponding author. E-mail: bgregg@nrel.nrel.gov.

<sup>⊗</sup> Abstract published in *Advance ACS Abstracts*, September 15, 1997.

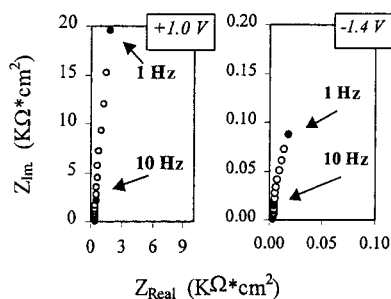


**Figure 1.** Typical real vs imaginary impedance spectra plots of high surface area  $\text{TiO}_2$  electrodes measured at 1 and  $-1.4$  V (vs SCE). The spectra were measured between 10 kHz and 1 Hz in acetonitrile, 0.3 M TBAPF<sub>6</sub> solution in the dark.

The films were then fired at 450 °C for 45 min in air, resulting in almost transparent electrodes.

Film thickness was measured with a computerized profilometer (Dektak 3), and the surface area was estimated by measuring the amount of sensitizing dye adsorbed to the films. The Ru(2,2'-bipyridine-4,4'-dicarboxylic acid)<sub>2</sub>(NCS)<sub>2</sub> dye (N3 from Solaronix SA) was adsorbed by immersing the electrodes overnight in a dry 0.5 mM ethanol solution of the dye.

**Measurements.** Impedance measurements (10 kHz to 1 Hz) were performed with Solartron 1287 Electrochemical Interface and 1260 Impedance/Gain Phase Analyzer. Zsim software (Scribner Associates) was used to model the impedance spectra. Other electrochemical measurements were performed with a PAR 173 potentiostat. Absorption spectra were measured with a HP 8452 spectrophotometer using an undyed  $\text{TiO}_2$  electrode as a reference. Scanning transmission measurements used a helium neon 5 mW laser (Melles Griot) tuned to 543 nm and a silicon diode (UDT instruments). The beam was focused down to approximately 40  $\mu\text{m}$  diameter.

All electrochemical experiments were done in a glovebox with a helium or nitrogen atmosphere using dry electrolytes. The electrolyte solution was 0.3 M tetrabutylammonium hexafluorophosphate (TBAPF<sub>6</sub>) in dry acetonitrile (ACN) except for one use of 0.3 M LiClO<sub>4</sub>. The acetonitrile (Burdick & Jackson) was dried and distilled over calcium hydride. All electrochemical measurements employed a three-electrode configuration. Potentials were measured vs ferrocene/ferrocenium (molar ratio 1:1) and are reported vs SCE. A two-compartment cell was designed for the impedance measurements. In this cell the  $\text{TiO}_2$  electrode was pressed against an O-ring to define its geometrical surface area and to avoid edge effects. The electrodes were not exposed to UV illumination prior to the electrochemical measurements in the dark. These conditions were found to be necessary for reproducibility, i.e., to obtain constant impedance at all potentials over more than 8 h.

## Results and Discussion

Impedance spectra of  $\text{TiO}_2$  nanoporous electrodes in electrolyte solution (0.3 M TBAPF<sub>6</sub>/ACN) were measured in the dark as a function of the applied potential and the  $\text{TiO}_2$  surface area. Figure 1 presents two typical impedance spectra (10 kHz to 1 Hz) measured at 1 and  $-1.4$  V. The measured spectra resemble the beginning of a large, slightly depressed semicircle. An equivalent electrical circuit that contained a solution resistor in series with a constant phase element (CPE) to model the electrode–electrolyte interface was used to fit the spectra.<sup>30</sup> The CPE used,  $Z = R/[1 + (i\omega RC)^\alpha]$ , is equivalent to a parallel resistor–capacitor (RC) circuit that produces a distribution of time constants. This distribution is modeled by the addition of an exponent ( $0 < \alpha < 1$ ) to the capacitor impedance. When a

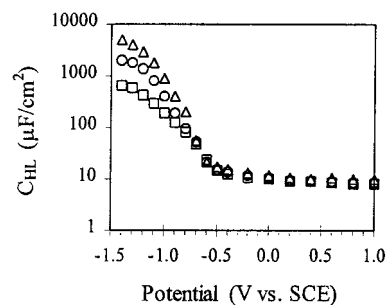


**Figure 2.** Capacitance of nanoporous  $\text{TiO}_2$  electrodes of different thickness as a function of the applied potential. The capacitance was extracted from impedance spectra measured in the dark using an electrical equivalent circuit (described in the text). The notation  $C_{\text{HL}}$ , which stands for the Helmholtz layer capacitance, will be justified later. ( $\square$ ) 0.6  $\mu\text{m}$ ; ( $\circ$ ) 2  $\mu\text{m}$ ; ( $\triangle$ ) 8  $\mu\text{m}$ .

single time constant is measured,  $\alpha$  equals unity and the CPE is equal to a normal parallel RC equivalent. However, when a nonuniform electrochemical response of the electrode generates a distribution of time constants,  $\alpha$  decreases as the distribution broadens. A distribution of time constants can result from either microscopic geometrical inhomogeneities or porosity that generates transmission line effects.<sup>31</sup>

The  $\text{TiO}_2$  electrode consists of sintered 15–25 nm colloids that cannot individually support a significant space charge layer.<sup>32</sup> However, a Helmholtz capacitance is expected at the  $\text{TiO}_2$ –electrolyte interface. In spite of the absence of a redox couple in the electrolyte solution in our experiments, a small amount of charge transfer (faradaic current) may still occur at this interface. A narrow distribution of time constants is expected to arise from the somewhat rough conducting  $\text{SnO}_2$  substrate, while a broader distribution is expected at the porous  $\text{TiO}_2$ –electrolyte interface. Therefore, the chosen CPE, which models a parallel circuit of a charge transfer resistor and a Helmholtz layer capacitor that have some distribution of time constants, is a good equivalent for this electrode–solution interface.

Excellent fits of the data to the model were obtained for all films. The following phenomena were observed for all scans: (1) the calculated solution resistance was constant throughout the potential range; (2) the interface resistance, calculated for the high surface area  $\text{TiO}_2$ , was larger than 200  $\text{k}\Omega/\text{cm}^2$ ; (3) the distribution of time constants ( $\alpha$ ) gradually changed from 0.95 at positive potentials to 0.8 when negative of  $-1.2$  V; and (4) the calculated capacitance changed significantly during the potential scan.

Figure 2 presents the calculated capacitance of the  $\text{TiO}_2$  electrodes as a function of the applied potential and the film thickness. When scanned negatively from +1 V, all films showed almost constant capacitance at first, followed by an increase of 2–3 orders of magnitude toward a plateau at negative potentials. The capacitance positive of  $\sim -0.5$  V was independent of film thickness and was comparable to the values of the bare conductive substrate. At potentials negative of  $\sim -0.5$  V, the measured capacitance was higher than the bare substrate, eventually increasing 2–3 orders of magnitude by  $-1.4$  V. Figure 3 shows that the capacitance of the different films becomes directly proportional to the films' surface area (expressed by the amount of dye adsorbed by these films after the capacitance measurements<sup>2</sup>) at  $-1.4$  V.

The behavior described above can be explained by the semiconducting nature of the  $\text{TiO}_2$  and the porous geometry of the films. Scheme 1 shows a simplified schematic view of the interconnected colloids represented as cross-linked columns. Electrolyte solution is able to penetrate through the  $\text{TiO}_2$  film

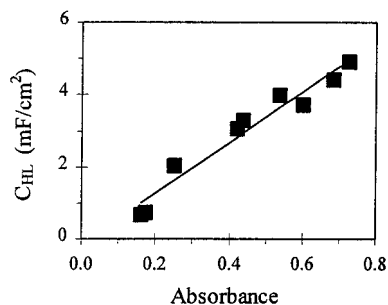
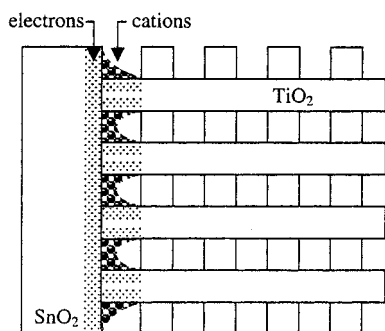


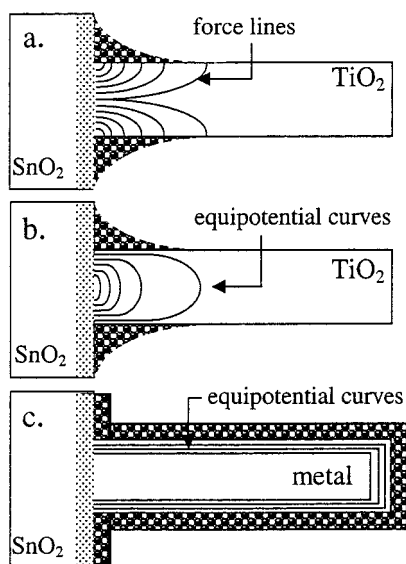
**Figure 3.** Capacitance of nanoporous TiO<sub>2</sub> films at  $-1.4$  V vs SCE (in the dark) as a function of the absorbance of these films when coated with dye. The absorbance is a measure of the films' surface area.

**SCHEME 1: Simplified Schematic View of the Nanoporous TiO<sub>2</sub> Films on the SnO<sub>2</sub> Substrate in Which the TiO<sub>2</sub> Is Represented as Columns<sup>a</sup>**



<sup>a</sup> As shown, a negative bias is applied to the SnO<sub>2</sub> electrode resulting in cation migration through the TiO<sub>2</sub> film to neutralize the applied electric field.

**SCHEME 2: Simplified Presentation of the Expected Electrical Force Lines (a) and Equipotential Curves (b) Generated in Porous TiO<sub>2</sub> Electrodes (Represented as Columns), When a Negative Potential Is Applied to the SnO<sub>2</sub> Substrate. (c) The Equipotential Curves Expected for a Similar, but Highly Conductive Electrode**



(columns) thus creating, under applied potential, a potential distribution unlike that in a compact electrode. A schematic representation of this unusual field distribution for one column is presented in Scheme 2. Parts a and b of Scheme 2 show, respectively, the approximate electric field force lines and the equipotential curves generated by a negative potential applied to such a representative semiconducting column immersed in

electrolyte solution. Scheme 2c shows the expected equipotential curves for a similar metallic or highly conducting column. In the latter case, there can be no potential drop across the metal; thus all the applied potential drops at the metal–solution interface. In contrast, when the porous film is insulating or semiconducting (Scheme 2a,b), the ability of the electrolyte ions to move toward the conducting substrate forces most of the potential to drop near the substrate. This implies that at increasing distance from the substrate, the semiconductor–solution potential difference decreases and, correspondingly, that the concentration of the electrons in the TiO<sub>2</sub> decreases. It is important to note that the difference in potential distribution between the metallic and the semiconducting cases results from their different conductivities relative to solution. In fact, this parameter determines the exact potential distribution for any given film geometry.

The TiO<sub>2</sub> films consist of weakly doped ( $\sim 10^{16}$  cm<sup>-3</sup>) colloids<sup>32</sup> and are therefore expected to approximate the semiconducting behavior of the above description (Scheme 2b). Electrons injected by the applied potential can, however, significantly increase the TiO<sub>2</sub> conductivity. Since the effect of the applied negative potential, and thus the electron concentration, decreases across the nanoporous film as the distance from the conductive substrate increases (Scheme 2b), a corresponding gradual change in the film's conductivity can be expected. Under negative bias, the TiO<sub>2</sub> nearest the substrate should become electrochemically active in the impedance measurements, while the outer part is still effectively insulating. The border between the two zones is anticipated to move away from the conductive substrate as the applied potential becomes more negative and a larger portion of the TiO<sub>2</sub> film becomes conductive. In other words, an increase in the electrochemically active surface area is expected when the applied bias is scanned negatively.

The impedance measurements described above show just such an increase in the effective surface area as the potential is scanned negatively. We attribute the measured capacitance to the Helmholtz layer capacitance ( $C_{HL}$ ). This capacitance is almost potential independent and is linearly dependent on the effective surface area.<sup>33</sup> At positive potentials the TiO<sub>2</sub> films are practically insulating, and therefore little or no contribution from the large TiO<sub>2</sub> surface area is observed. The overall capacitance at positive potential is due to the  $C_{HL}$  of the exposed conducting substrate and a few monolayers of TiO<sub>2</sub>. Only when the TiO<sub>2</sub> is “doped”, by application of a negative bias, does it become conductive and therefore electrochemically active. This results in the observed increase of the capacitance (effective surface area) toward a plateau at the potential where the entire surface area of the film is active. At  $-1.4$  V, when the major part of the nanoporous film becomes electrochemically active, a direct proportionality between the capacitance and the surface area is observed (Figure 3).

The change in the calculated distribution of time constants ( $\alpha$ ) during the potential scan also supports this interpretation. The distribution broadens during the negative sweep as reflected by the decrease of  $\alpha$  from 0.95 to 0.8. The broadening of the time constant distribution indicates an increase of the effective electrode roughness.<sup>30</sup> At positive potentials when only the conductive substrate is electrochemically active, a narrow time constant distribution is observed ( $\alpha \rightarrow 1$ ). However, as the porous film becomes electrochemically active at negative bias, the effective roughness increases and therefore the distribution broadens ( $\alpha \rightarrow 0.8$ ).

It is important to note that in these experiments the steady-state currents, measured for the entire TiO<sub>2</sub> surface area, were

lower than 20 nA/cm<sup>2</sup> even at -1.4 V, and the calculated interface resistances were higher than 200 kΩ/cm<sup>2</sup>. These conditions confirm that the measured phenomena do not result from voltage drops that are caused by current flow through resistive materials (*iR* drops), but rather by the basic properties of these electrodes.

An alternative interpretation of the impedance results was considered, but eliminated. It would attribute the observed increase in capacitance at negative potentials to the accumulation layer capacitance ( $C_{AL}$ ), which has a strong potential dependence:<sup>34</sup>

$$C_{AL} = (q^2 N_D \epsilon \epsilon_0 A^2 / 2kT)^{1/2} \exp(-qVs/2kT) \quad (1)$$

where  $q$  is the elementary charge,  $N_D$  is the doping density,  $\epsilon_0$  is the vacuum permittivity,  $\epsilon$  is the TiO<sub>2</sub> dielectric constant,  $A$  is the film surface area,  $kT$  are the Boltzman constant and the temperature, and  $Vs$  is the bias beyond the flat band potential. Since the accumulation layer is in series with  $C_{HL}$ , only the smaller capacitance of the two can be detected. In this interpretation, the impedance results would be explained as an exponential increase in  $C_{AL}$  with potential, followed by a plateau attributed to constant  $C_{HL}$  once  $C_{AL}$  becomes larger than  $C_{HL}$ . However, this interpretation could not explain four major observations: (1) the measured capacitance is much smaller than  $C_{AL}$  calculated by eq 1; (2) the measured slope of the capacitance vs potential negative of  $\sim -0.5$  V ranges between 255 and 458 mV per decade capacitance, while eq 1 requires a slope of 120 mV; (3) according to eq 1 the slope of the capacitance vs applied bias should not be affected by a change of the electrode surface area, yet the measured slopes show a strong dependence on the film thickness (Figure 2); and (4) no change in the distribution of time constants at the semiconductor-electrolyte interface ( $\alpha$ ) as a function of the applied potential should be observed. For these reasons we can eliminate this alternative explanation and conclude that the measured capacitance indeed represents  $C_{HL}$  and not  $C_{AL}$ .

An independent and unambiguous measure of the potential distribution in the TiO<sub>2</sub> nanoporous electrodes is provided by electrochemical dye desorption experiments. Dyes are desorbed from the TiO<sub>2</sub> film above a threshold negative potential,<sup>9</sup> providing a means to directly visualize the spatial variation in the potential distribution by absorbance measurements. If the applied negative potential decreases across the film as proposed above, the dye should desorb only near the conductive substrate under moderate negative bias.

A special electrode was designed to enable absorbance measurements as a function of the distance from the electrical contact. A 4 μm thick TiO<sub>2</sub> film was deposited on a nonconductive glass and a silver contact was evaporated at one end of the film (see insert in Figure 4). The electrode was immersed in the electrolyte solution in a three-electrode cell, exposing part of the silver contact to the solution. To ensure steady-state conditions, the negative potential was applied for 10 min while the solution was stirred. After the electrochemical desorption the films were rinsed and dried, and the transmission along the electrodes was measured with a 40 μm laser spot at 543 nm. An undyed similar film was used to define the transmission baseline.

Figure 4 presents the normalized transmission of the TiO<sub>2</sub> films as a function of the distance from the edge of the silver contact at different applied potentials. When the laser spot is scanned along the metal contact, the light is fully reflected (distance < 0). Right next to the contact the transmission approaches unity indicating that the dye completely desorbed in this region, followed by a transmission decay to 0 as the

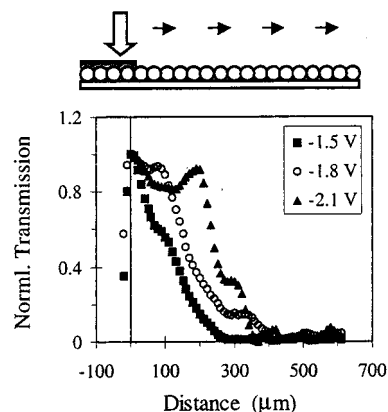


**Figure 4.** Normalized transmission along dye-coated TiO<sub>2</sub> films that were exposed to the indicated potentials in acetonitrile, 0.3 M TBAPF<sub>6</sub> solution in the dark. The transmission was normalized by considering the transmission of an undyed film as 1 and the transmission of the fully dyed film as 0. The transmission was measured at 543 nm with a 40 μm laser beam. A cross section of the electrode and the illumination is shown as an insert.

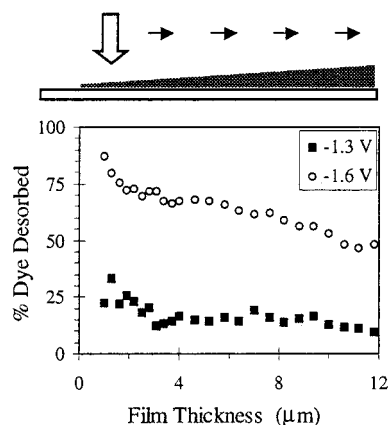


**Figure 5.** Percentage of the dye that desorbed at the indicated potentials as a function of the film thickness. The electrochemical desorption was done in acetonitrile, 0.3 M TBAPF<sub>6</sub> solution in the dark. The transmission was measured with a 40 μm laser beam. A cross section of the electrode and the illumination is shown as an insert.

spot is scanned toward the region where the dye concentration was unaffected by the applied potential. Since the dye desorbs only where the TiO<sub>2</sub> reaches a sufficiently negative potential, this experiment shows directly that the potential near the contact is more negative than the potential further away from the contact. The width of the region where the dye desorbed completely increases at more negative biases (Figure 4), illustrating the penetration of the desorption threshold potential into the film.

The regular electrodes (thin TiO<sub>2</sub> films deposited on conducting substrates) behave in a similar way. Dye desorption from this type of electrode is completed only 300–800 mV negative of the potential required to initiate dye desorption. To ensure that this behavior does not result from a distribution of dye-TiO<sub>2</sub> binding energies, an electrode with a TiO<sub>2</sub> film thickness gradient was made (see insert in Figure 5). The absorbance of the film before and after the electrochemical dye desorption experiments was measured, yielding the percentage of desorbed dye as a function of film thickness. Figure 5 shows that at a given potential there is an inverse relationship between the fraction that desorbs and the film thickness. This observation is consistent with the limited penetration depth of the desorption threshold potential, which reaches an increasing fraction of the film as the latter becomes thinner.

The low conductivity of the nanoporous TiO<sub>2</sub> film plays a major role in the potential distribution described earlier. A more

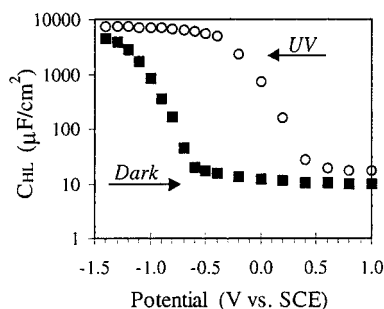


**Figure 6.** Capacitance of nanoporous TiO<sub>2</sub> electrode in the dark and under UV illumination as a function of the applied potential. The capacitance was extracted from impedance spectra using the electrical equivalent circuit described in the text.

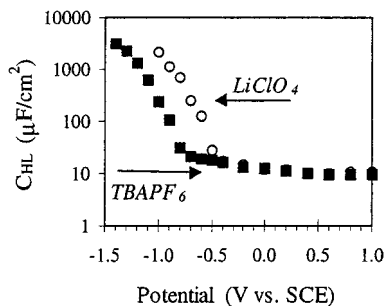


**Figure 7.** Capacitance of a nanoporous TiO<sub>2</sub> electrode in acetonitrile 0.3 M TBAPF<sub>6</sub> and LiClO<sub>4</sub> solutions as a function of the applied potential. The capacitance was extracted from impedance spectra (measured in the dark) using the electrical equivalent circuit described in the text.

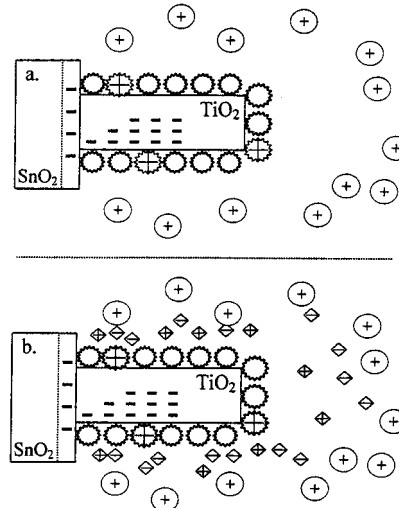
conductive semiconductor is expected to show a behavior approaching that in Scheme 2c. Ultraviolet illumination can increase the TiO<sub>2</sub> conductivity by more than 6 orders of magnitude<sup>28</sup> enabling examination of the effect of the conductivity on the potential distribution. Figure 6 presents the capacitance of a film at different potentials, before and during illumination. The threshold potential for capacitance increase is shifted positively by approximately 1 V upon illumination, and a clear plateau over a range of 0.8 V is observed. Figure 6 clearly shows that when a given bias is applied, the effective surface area is determined by the conductivity of the porous electrode. For example, at  $-0.5$  V when the electrode is nonconductive (dark), only the conductive substrate and the nearest layers of TiO<sub>2</sub> appear electrochemically active. However, under the same applied bias, when the electrode is made conductive by ultraviolet illumination, the electrochemically active surface area of the electrode is equal to the geometrical surface area.

The presence of lithium ions in the electrolyte solution also seems to make the TiO<sub>2</sub> more conductive at a given potential. Figure 7 presents the capacitance vs voltage curve of an electrode first measured with 0.3 M TBAPF<sub>6</sub> in acetonitrile followed by a measurement in 0.3 M LiClO<sub>4</sub> solution. As in the case of UV illumination, we attribute the positive shift of the threshold potential to the increase in the TiO<sub>2</sub> conductivity upon exposure to LiClO<sub>4</sub> solution. This may result from either a positive shift of the conduction band or from lithium intercalation.<sup>36</sup>

### Implications for Dye-Sensitized Solar Cells

In the previous section the unusual potential distribution across the porous semiconducting electrode was discussed. In this section, we discuss some implications of this result to the operation of dye-sensitized solar cells.

### SCHEME 3: Photoinduced Charge Separation Process Creates an Electrostatic Field between the Injected Electrons (Shown as $-$ in the TiO<sub>2</sub>) and the Resulting Uncompensated Cations (Shown as $\oplus$ in the Solution)<sup>a</sup>



<sup>a</sup> This electrostatic field opposes the charge separation processes. (a) In the absence of mobile supporting electrolyte, the photoinduced electric field promotes charge recombination. (b) Mobile supporting electrolyte screens the photoinduced field allowing efficient charge separation to occur.

Upon illumination of a dye-sensitized solar cell, an electron is injected from the dye into the TiO<sub>2</sub> film and a hole is transferred to the electrolyte. The injected electrons have to cross the TiO<sub>2</sub> film and reach the conducting substrate, while the oxidized ions diffuse toward the back electrode where they are rereduced. The mechanism by which injected electrons move through the TiO<sub>2</sub> film is important to the overall understanding of the system. Models describing electron motion as a diffusion process have been developed in some studies,<sup>21,37</sup> and good agreement with the experimental current response to light modulation was obtained. However, these studies did not provide a clear rationale for the assumption of diffusion as the transport mechanism.

The results described above provide this rationale. Because of the porous nature of the TiO<sub>2</sub> film, ions can migrate through the film to neutralize any electric fields (including those caused by photo injected electrons) over very short distances. Therefore, under normal operating conditions, there should be essentially no macroscopic electric fields (of range longer than about 20–50 nm<sup>33</sup>) in the TiO<sub>2</sub> film, depending on the electrolyte concentration and composition. Accordingly, during steady-state illumination, the injected electrons will experience little or no electric field, so their motion will be governed primarily by concentration gradients; that is, it will be diffusional.

Since there are essentially no electric fields present in the dark, a transient electric field (image force) will be created by the photoinjection process upon illumination. Scheme 3a illustrates these electric fields which result from the opposing movement of electrons and holes (oxidized ions). The photoinduced field will oppose further charge separation and promote charge recombination. The presence of mobile ions in the film, however, can mitigate this field-induced recombination process. As discussed earlier, the mobile ions can constantly rearrange to screen these photoinduced electrostatic fields. Scheme 3b illustrates the anticipated steady-state system configuration, in which the photoinduced fields are screened by the electrolyte, that enables the efficient charge separation achieved in recent dye-sensitized solar cells.<sup>3</sup>

The transient fields created upon illumination should not be important for steady-state processes. However, they may have a marked influence on time-resolved measurements. For example, the driving force for the recombination reaction between electrons in the TiO<sub>2</sub> and the oxidized dye or acceptor in solution is expected to decrease with time after a laser flash as the photoinduced electric field is neutralized. Time-resolved measurements made on electrodes in solution may, therefore, be qualitatively different from those made on dry ones.

The solid-state analogues of dye-sensitized solar cells proposed and studied so far did not contain mobile electrolyte ions.<sup>13,14</sup> The conversion efficiency in such systems has been uniformly low. One reason for this low efficiency may have been the photoinduced, uncompensated electric fields in these cells that oppose the charge separation (Scheme 3a). It should be possible, however, to design a solid-state version of the dye-sensitized cells that contains mobile electrolyte ions that will eliminate this problem. Such experiments are in progress.

### Conclusions

The high surface area TiO<sub>2</sub> electrodes that are used mainly for dye-sensitized cells enable electrolyte ions to migrate throughout the film. As a consequence, during steady-state operation there are essentially no macroscopic electric fields in these cells. This field screening may have several implications for the functioning of dye-sensitized solar cells: (1) Charge carrier motion through the TiO<sub>2</sub> is expected to occur primarily via diffusion rather than drift. (2) Illumination of a system initially at equilibrium will result in transient generation of an electric field between the injected electrons and the oxidized solution species. This transient electric field will be quickly neutralized under steady state conditions, but may be an important factor in non steady state measurements. (3) Systems that do not contain excess supporting electrolyte, such as some solid state versions of the dye-sensitized cells, may not be able to efficiently neutralize the field generated by the photoinduced charge separation. Therefore, charge recombination rather than charge separation may dominate in such systems.

The field neutralization effect was extracted from impedance spectra and electrochemical dye desorption measurements. These measurements show that, because of the ability of the ions to neutralize the electric fields coupled with the low conductivity of the TiO<sub>2</sub>, the potential of much of the TiO<sub>2</sub> film will not necessarily correspond to the potential applied to the substrate electrode. This unusual potential distribution should be considered when such electrodes are tested by electrochemical methods.

**Acknowledgment.** We are grateful to the U.S. Department of Energy for funding this research. A.Z. was supported by the Office of Energy Efficiency and Renewable Energy, Office of Utility Technologies, Photovoltaics Division. A.M. and B.G. were supported by the Office of Energy Research, Division of Basic Energy Science, Chemical Sciences Division.

### References and Notes

- (1) O'Regan, B.; Grätzel, M. *Nature* **1991**, *353*, 737–740.

- (2) Nazeeruddin, M. K.; Kay, A.; Rodicio, I.; Humphry-Baker, R.; Muller, E.; Liska, P.; Vlachopoulos, N.; Grätzel, M. *J. Am. Chem. Soc.* **1993**, *115*, 6382–6390.
- (3) Grätzel, M. Presented at the First Conference on Future Generation Photovoltaic Technologies, Denver, CO, 1997.
- (4) Memming, R. *Photochem. Photobiol.* **1972**, *16*, 325–333.
- (5) Gerischer, H. *Photochem. Photobiol.* **1972**, *16*, 243–260.
- (6) Parkinson, B. A.; Spittler, M. T. *Electrochim. Acta* **1992**, *37*, 943–948.
- (7) Zaban, A.; Ferrere, S.; Sprague, J.; Gregg, B. A. *J. Phys. Chem.* **1997**, *101*, 1, 55–57.
- (8) Huang, S. Y.; Schlichthörl, G.; Nozik, A. J.; Grätzel, M.; Frank, A. J. *J. Phys. Chem. B* **1997**, *101*, 2576–2582.
- (9) Kamat, P. V.; Bedja, I.; Hotchandani, S.; Patterson, L. K. *J. Phys. Chem.* **1996**, *100*, 4900–4908.
- (10) Argazzi, R.; Bignozzi, C. A.; Heimer, T. A.; Meyer, G. J. *Inorg. Chem.* **1997**, *36*, 2–3.
- (11) Burfeint, B.; Hannappel, T.; Storck, W.; Willig, F. *J. Phys. Chem.* **1996**, *100*, 0, 16463–16465.
- (12) Hagfeldt, A.; Didriksson, B.; Palmqvist, T.; Lindstrom, H.; Sodergren, S.; Rensmo, H.; Lindquist, S.-E. *Sol. Energy Mater. Sol. Cells* **1994**, *31*, 481–488.
- (13) O'Regan, B.; Schwartz, D. T. *J. Appl. Phys.* **1996**, *80*, 4749–4754.
- (14) Tennakone, K.; Kumara, G. R. R. A.; Kumarasinghe, A. R.; Wijayantha, K. G. U.; Sirimanne, P. M. *Semicond. Sci. Technol.* **1995**, *10*, 1689–1693.
- (15) Fessenden, R. W.; Kamat, P. V. *J. Phys. Chem.* **1995**, *99*, 12902–12906.
- (16) Ferrere, S.; Zaban, A.; Gregg, B. A. *J. Phys. Chem. B*, **1997**, *101*, 4490–4493.
- (17) Bechinger, C.; Ferrere, S.; Zaban, A.; Sprague, J.; Gregg, B. A. *Nature* **1996**, *383*, 608–610.
- (18) Gregg, B. A. *Endeavour* **1997**, *21*, 52–55.
- (19) Gerfin, T.; Grätzel, M.; Walder, L. In *Molecular Level Artificial Photosynthetic Materials*; Meyer, G. J., Ed.; John Wiley & Sons: New York, 1997.
- (20) Lindstrom, H.; Rensmo, H.; Sodergren, S.; Solbrand, A.; Lindquist, S.-E. *J. Phys. Chem.* **1996**, *100*, 3084–3088.
- (21) Cao, F.; Oskam, G.; Meyer, G. J.; Searson, P. C. *J. Phys. Chem.* **1996**, *100*, 17021–17027.
- (22) Boschloo, G. K.; Goossens, A. *J. Phys. Chem.* **1996**, *100*, 19489–19494.
- (23) Fitzmaurice, D. *Sol. Energy Mater. Sol. Cells.* **1994**, *32*, 289–305.
- (24) Dolata, M.; Kedzierzawski, P.; Augustynski, J. *Electrochim. Acta* **1996**, *41*, 1287–1293.
- (25) Cao, F.; Oskam, G.; Searson, P. C.; Stipkala, J. M.; Heimer, T. A.; Farzad, F.; Meyer, G. J. *J. Phys. Chem.* **1995**, *99*, 11974–11980.
- (26) Lemon, B. I.; Hupp, J. T. *J. Phys. Chem.* **1996**, *100*, 14578–14580.
- (27) Doherty, S.; Fitzmaurice, D. *J. Phys. Chem.* **1996**, *100*, 10732–10732.
- (28) Rashti, M. A.; Brodie, D. E. *Thin Solid Films* **1994**, *240*, 163–167.
- (29) Konenkamp, R.; Hennigner, R.; Hoyer, P. *J. Phys. Chem.* **1993**, *97*, 7328–7330.
- (30) MacDonald, J. R. *Impedance Spectroscopy*; John Wiley & Sons: New York, 1987.
- (31) Gabrielli, C. *Identification of Electrochemical Processes by Frequency Response Analyzer*; Publication No. 004/83; Schlumberger Solartron Electronic Group Ltd., 1990.
- (32) O'Regan, B.; Moser, J.; Anderson, M.; Grätzel, M. *J. Phys. Chem.* **1990**, *94*, 8720–8726.
- (33) Bard, A. J.; Faulkner, L. R. *Electrochemical Methods Fundamental and Applications*; John Wiley & Sons: New York, 1980.
- (34) Morrison, S. R. *Electrochemistry at Semiconductor and Oxidized Metal Electrodes*; Plenum Press: New York, 1980; Chapter 4.
- (35) Andrew, L. A.; Hupp, J. T. *J. Phys. Chem.* **1995**, *99*, 15718–15720.
- (36) Sodergren, S.; Hagfeldt, A.; Olsson, J.; Lindquist, S.-E. *J. Phys. Chem.* **1994**, *98*, 5552–5556.